RSC Advances

PAPER

View Article Online
View Journal | View Issue

Cite this: *RSC Adv.*, 2018, **8**, 16146

Label-free impedimetric sensing platform for microRNA-21 based on ZrO_2-reduced graphene oxide nanohybrids coupled with catalytic hairpin assembly amplification†

Keying Zhang,* Na Zhang, Li Zhang, Hongyan Wang, Hongwei Shi and Qiao Liu

Received 21st March 2018
Accepted 16th April 2018

DOI: 10.1039/c8ra02453g

rsc.li/rsc-advances

Herein, a sensitive electrochemical impedance sensor was constructed based on ZrO_2-reduced graphene oxide (RGO)-modified electrode coupled with the catalytic hairpin assembly signal amplification strategy. Electrochemical impedance spectroscopy (EIS) was used to detect microRNA (miRNA) using the change in electron transfer resistance (ΔR_{et}) originated from nucleic acid hybridization on the electrode surface. MiRNA-21 was used as a model to verify this strategy. The results indicated that ΔR_{et} exhibited a good linear relationship with the concentration of miRNA-21 in the range from 1.0×10^{-14} mol L^{-1} to 1.0×10^{-10} mol L^{-1} with a detection limit of 4.3×10^{-15} mol L^{-1} (S/N = 3). Additionally, this sensor exhibited good selectivity, and it could be applied to detect miRNA-21 in human serum samples and measure the expression levels of miRNA-21 in human breast cancer cell lines (MCF-7); thus, this sensor has great potential in cancer diagnosis.

1 Introduction

The abnormal expression of microRNAs, which are used as tumour biomarkers, is related to various diseases such as cancers. Therefore, the development of reliable methods for detecting miRNA has been paid great attention to, and various methods have been developed such as fluorescence,[1,2] radiochemistry,[3] surface plasmon resonance spectroscopy,[4] and electrochemistry.[5–9] Among these methods, electrochemical sensors have been widely paid attention to due to their merits including quick response, high sensitivity and selectivity, low cost, and easy microminiaturization.[10–12] However, a few challenges still exist; for example, probes need be labelled in the preparation of some sensors, which is very time-consuming and expensive. Thus, label-free electrochemical nucleic acid sensors are extremely desirable.

The construction of electrochemical impedance biosensor is a convenient technique for label-free nucleic acid detection. Several groups have successfully constructed label-free electrochemical impedance nucleic acid sensors. For example, Jiao *et al.* reported a poly(xanthurenic acid)-RGO nanocomposite for highly sensitive impedimetric detection of DNA.[13] Li *et al.* constructed a label-free DNA biosensor based on enhanced charge transfer by gold nanoparticles.[14]

Nanomaterials having excellent biocompatibility have been considered as attractive materials to construct modified electrodes due to their unique structural, electronic, magnetic, optical and catalytic properties.[15–17] ZrO_2, a thermally stable inorganic oxide, shows lack of toxicity and affinity for the groups containing oxygen;[18,19] thus, it is an ideal material for biomolecules with oxygen group immobilization. Recently, many ZrO_2-based electrochemical DNA sensors have been reported. Liu *et al.*[20] described a method of immobilizing DNA based on the sol–gel technique. Jiao *et al.* reported a synergistic membrane of ZrO_2/self-doped polyaniline nanofibres for DNA hybridization detection.[21] Fang *et al.* reported a ZrO_2 thin film-modified electrode for DNA hybridization detection.[22] Wang *et al.* reported a sphere-like CeO_2–ZrO_2 and chitosan nanocomposite-modified electrode for DNA detection.[23] Despite the fact that the ZrO_2 film can provide an ideal interface for the immobilization of the DNA probe, which improves the detection sensitivity, the sensitivity of the nucleic acid sensor still needs be improved to meet the need of the low-abundance miRNA detection.

Recently, benefiting from molecular programming, enzyme-free DNA circuits for amplifying signals by governing the simple rules of DNA hybridization have been developed in miRNA detection such as hybridization chain reaction (HCR),[24,25] catalyzed hairpin assembly (CHA),[26,27] and entropy-driven catalysis.[28,29] CHA shows great potential in signal amplification, and

Anhui Key Laboratory of Spin Electron and Nanomaterials, School of Chemistry and Chemical-Engineering, Suzhou University, Suzhou, Anhui 234000, People's Republic of China. E-mail: zhangky1983@163.com

† Electronic supplementary information (ESI) available: Cell culture; miRNA-21 extracts from cancer cells; TEM and EDX of ZrO_2-RGO; the optimization of hybridization time; the nucleic acid sequences; comparison of linear range and detection limit of the reported sensors; determination results of miRNA-21 in human serum. See DOI: 10.1039/c8ra02453g

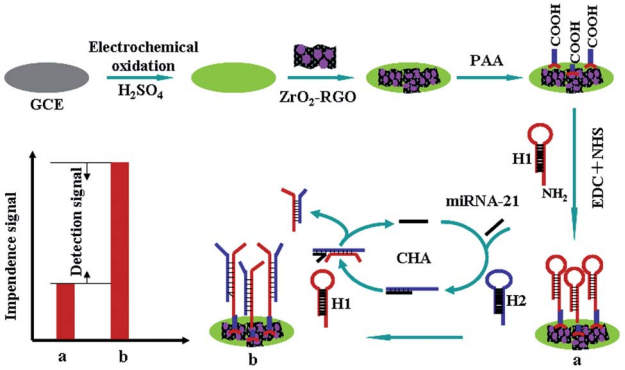

Scheme 1 Schematic representation of the immobilization of probe and miRNA-21 detection.

a cascade of hybridization reactions can be triggered to release the target miRNA, resulting in high sensitivity for the detection of target molecules. Thus, a combination of the electrochemical impedance technique and sensitivity of the CHA amplification strategy is ideal for highly sensitive miRNA detection.

Herein, we presented a highly sensitive electrochemical impendence sensor based on ZrO_2-RGO-modified electrode coupled with the CHA signal amplification strategy (Scheme 1). The change in electron transfer resistance ($\Delta R_{et} = \Delta R_{et}$ (b) $- \Delta R_{et}$ (a)) originating from nucleic acid hybridization on the electrode surface was used as a signal to measure target miRNA. The CHA strategy consists of two hairpin DNA molecules (H1 and H2) (in this study, all the nucleic acid sequences are listed in Table S1†). Prior to ZrO_2-RGO modification, the glassy carbon electrode (GCE) with the oxygen functional group was obtained by an electro-oxidation process according to the previously reported process,[30] and this provided a suitable interface for ZrO_2-RGO modification through the reaction between the oxygen functional group and ZrO_2.[22] H1 modified with an amino-group was covalently bonded onto the ZrO_2-RGO-modified GCE surface *via* poly(acrylic acid) (PAA, MW, 2000) with the aid of *N*-(3-(dimethylamino) propyl)-*N*-ethyl-carbodiimide hydrochloride (EDC) and *N*-hydroxysuccinimide (NHS). In the absence of miRNA, H1 and H2 could not react with each other and thus, ΔR_{et} exhibited no obvious change. When a copy of target miRNA is present, hairpin of H2 is opened by hybridizing to the target miRNA; H1 then hybridizes with the unfolded H2, and the target miRNA is released based on the DNA strand displacement reaction. Finally, H2 was immobilized onto the electrode surface. After that, the released target miRNA initiated the next cycles, as a result of which numerous H2 molecules were immobilized onto the electrode surface, which amplified the detection signal. Thus, target miRNA could be detected with high sensitivity. To verify this strategy, miRNA-21 was used as a model, and the results indicated that this method had good selectivity and could detect miRNA-21 in human serum samples. Importantly, this method was employed to successfully measure the expression levels of miRNA-21 in MCF-7 cells and thus, it has great potential in cancer diagnosis.

2 Experimental

2.1 Reagents and apparatus

$ZrOCl_2 \cdot 8H_2O$, *N*-(3-(dimethylamino) propyl)-*N*-ethyl-carbodiimide hydrochloride (EDC), *N*-hydroxysuccinimide (NHS), and poly(-acrylic acid) (MW, 2000) were purchased from Alfa Aesar (Tianjing, China). RGO was purchased from Chengdu Institute of Organic Chemistry, Chinese Academy of Sciences and used without further purification. All chemicals were of analytical grade and used without further purification. All solutions were prepared with doubly distilled water. All the nucleic acid sequences were purchased from Shanghai Sangon Bioengineering (Shanghai, China). Stock solutions of nucleic acid were prepared with Tris–HCl (20 mM, pH 7.4, 5 mM $MgCl_2$, 50 mM NaCl), and they were stored in a freezer.

Electrochemical impedance tests were carried out on the CHI660d electrochemical workstation (Shanghai Chenhua Instruments, China). The three-electrode system was used in the experiment with bare GCE or modified electrode as the working electrode, a saturated calomel electrode (SCE) as the reference electrode, and a platinum wire as the counter electrode. Electrochemical impedance spectroscopy (EIS) was performed in 0.1 M PBS (pH 7.4, 0.1 M NaCl) in the presence of 5 mM $[Fe(CN)_6]^{3-/4-}$ as a redox probe in the frequency range between 0.01 and 10^5 Hz at the formal potential of 0.2 V. The AC voltage amplitude was 5 mV. All electrochemical measurements were carried out in a 10 mL electrochemical cell, from which oxygen was removed using high-purity nitrogen for 15 min, and a blanket of nitrogen was maintained over the solutions during the measurements.

Polyacrylamide gel electrophoresis (PAGE) analysis was carried out using a Bio-Rad electrophoresis analyzer (USA) and images were obtained on Bio-Rad ChemDoc; a Hitachi S-3000 N scanning electron microscope (SEM, Japan) was also utilized. XRD measurements were performed on a Japan Shimadzu XRD-6000 diffractometer with Cu-Kα radiation ($\lambda = 0.15418$ nm) and a scanning rate of 0.05 deg s^{-1} TEM measurements were carried out on a JEOL-2100 instrument with an acceleration voltage of 200 kV. In this study, informed consents were obtained from human participants.

2.2 Fabrication of H1/PAA/ZrO_2-RGO/GCE

Bare GCE was polished to obtain a mirror-like surface with 1.0, 0.3, and 0.05 μm alumina slurries; it was thoroughly rinsed with water and sonicated in nitric acid (1 : 1), acetone and doubly distilled water (each for 1 min). The electrode was then oxidized by performing 10 cycles in 0.1 mol L^{-1} H_2SO_4 between 0 and +2.0 V at the scan rate of 0.1 V s^{-1}.[30] ZrO_2-RGO nanohybrids were prepared according to our previously reported method.[31] ZrO_2-RGO (1.0 mg) was dispersed in 10 mL DMF by ultrasonic agitation for about 40 min to get a 0.1 mg mL^{-1} suspension. ZrO_2-RGO suspension (10 μL) was dropped onto the fresh GCE surface and dried naturally at room temperature; it was then immersed into doubly distilled water for 5 min and washed with doubly distilled water three times to remove loosely adsorbed ZrO_2-RGO. ZrO_2-RGO/GCE was then put into 0.1 mol L^{-1} PAA

solution for 12 h. After washing, PAA/ZrO_2-RGO/GCE was immersed into PBS containing 20.0 mg mL^{-1} EDC, 10.0 mg mL^{-1} NHS, and 1.0 μM H1 at the room temperature for 4 h, which was followed by rinsing with Tris–HCl; H1/PAA/ZrO_2-RGO/GCE was thus fabricated.

2.3 Electrochemical detection of DNA hybridization

Hybridization was carried out by immersing H1/PAA/ZrO_2-RGO/GCE into Tris–HCl solution containing target miRNA and 0.1 μM H2 for 50 min at 37 °C; the electrode was then rinsed with Tris–HCl, and the electrochemical impedance tests were performed.

3 Results and discussion

3.1 The characterization of ZrO_2-RGO

Scanning electron microscopy (SEM) was used to characterize ZrO_2-RGO. SEM images of RGO (A) and ZrO_2-RGO (B) are shown in Fig. 1. A clear change was observed between the morphologies of RGO and ZrO_2-RGO. Compared with the observations for RGO, many nanoparticles were modified onto the ZrO_2-RGO surface, indicating the formation of ZrO_2-RGO nanohybrids. X-ray powder diffraction (XRD) was used to confirm the above-mentioned result. As shown in Fig. 1C, the typical peaks of 24.2° were indexed as RGO;[32] the other typical peaks were indexed as the monoclinic and tetragonal ZrO_2. These peaks matched the standard JCPDS data no. 00-037-1484 and 01-079-1769, indicating that the prepared ZrO_2 comprised monoclinic and tetragonal ZrO_2. Energy dispersive X-ray spectroscopy (EDX) and transmission electron microscopy (TEM) were used to further confirm the formation of ZrO_2-RGO nanohybrids (Fig. S1†). The above-mentioned results agreed well with those of the previous report,[33] indicating that ZrO_2-RGO nanocomposites were successfully synthesized.

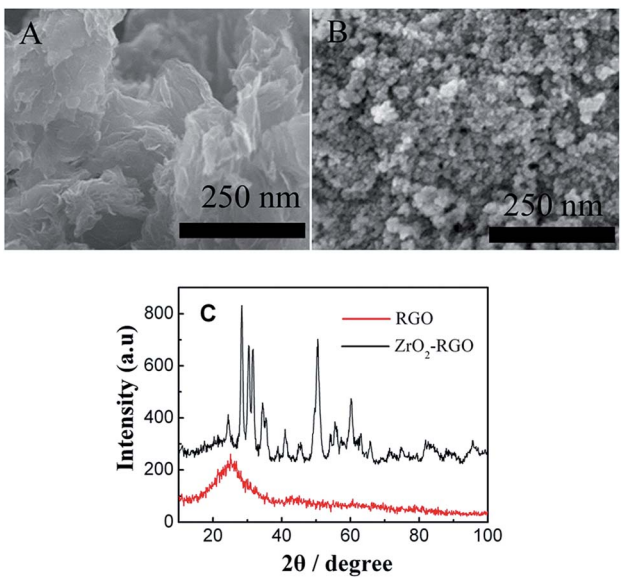

Fig. 1 SEM images of RGO (A) and ZrO_2-RGO (B). XRD patterns of RGO and ZrO_2-RGO nanohybrids (C).

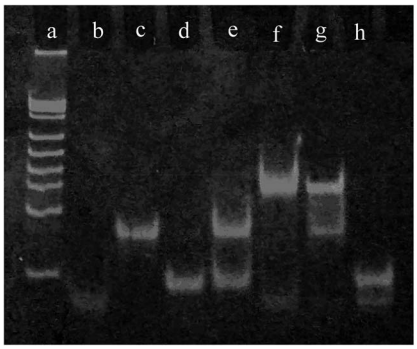

Fig. 2 The PAGE analysis: reference ladder (a), miRNA-21 (b), H2 (c), H1 (d), H2 + H1 (e), H2 + miRNA-21 + H1 (f), H2 + miRNA-21 (g), and miRNA-21 + H1 (h). Voltage: 100 V; time: 1 h.

3.2 The feasibility of this design

The PAGE (12%) experiment was used to investigate the feasibility of this design. As shown in Fig. 2, a band was observed at different positions with just H2 or H1 in the solution (lane c and d, respectively). Two bands were observed in the mixture of H2 and H1 (lane e); they were the same as those for H2 or H1, indicating that H1 and H2 cannot react with each other. When miRNA-21 was added into the H2 solution, a new band appeared, and the band of miRNA-21 disappeared (lane g). After H1 was added into the mixture of miRNA-21 and H2, the band of H2 disappeared, and a new band and a miRNA-21 band appeared (lane f). In addition, miRNA-21 and H1 could not react with each other (lane h). These above-mentioned results illustrated that target miRNA-21 can serve as a catalyst to activate the hairpin assembly reaction and to amplify the signal.

3.3 Immobilization of the sensor

Fig. 3 shows EIS of different electrodes. In EIS, the semicircle diameter corresponds to the electron transfer resistance (R_{et}). A small R_{et} was observed at bare GCE. After ZrO_2-RGO was modified onto the electrode surface, R_{et} increased. Upon comparison of the spectra of different electrodes, it was

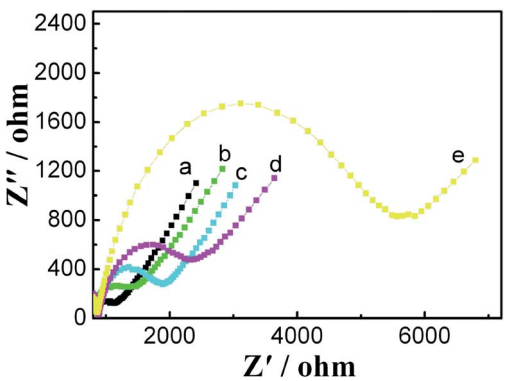

Fig. 3 Impedance spectra of bare GCE (a), ZrO_2-RGO/GCE(b), PAA/ZrO_2-RGO/GCE(c), H1/PAA/ZrO_2-RGO/GCE (d), and H2/H1/PAA/ZrO_2-RGO/GCE (e).

observed that R_{et} increased after H1 was immobilized, which was ascribed to the negatively charged phosphate backbone of H1 on the electrode surface repelling $[Fe(CN)_6]^{3-/4-}$ anions; this indicated that H1 was successfully modified onto the electrode surface. In the presence of 0.1 nM miRNA-21, R_{et} further increased, because the negative charge increased on the electrode surface due to the formation of H2/H1. These above-mentioned results indicated that the proposed sensor can be successfully prepared, and it exhibits response to miRNA-21.

3.4 The sensitivity and selectivity

The optimum hybridization time was investigated. The results showed that 50 min was the optimal time (Fig. S2†). Under optimum experimental conditions, the sensitivity and selectivity of the sensor were studied. Fig. 4 shows that ΔR_{et} increased with an increase in the concentration of miRNA-21. ΔR_{et} was linear with the logarithm of the concentration of miRNA-21 in the range from 1.0×10^{-14} mol L^{-1} to 1.0×10^{-10} mol L^{-1}. The regression equation was $\Delta R_{et} = 9949.6 + 684.2 \log c_{miRNA\text{-}21}$ ($R = 0.9902$), and the detection limit was 4.3×10^{-15} mol L^{-1} (S/N = 3). The performances of this sensor were compared with those of some previously reported sensors (Table S2†), indicating that this sensor shows excellent performance.

The selectivity of the sensor was investigated by measuring ΔR_{et} obtained for hybridizing with various kinds of miRNA (Fig. 5). No significant changes in ΔR_{et} were observed between the blank solution and the solutions containing miRNA-141 and three-base mismatched miRNA-21 (t-miRNA-21). However, an increase in ΔR_{et} was observed after miRNA-21 was added, indicating that the sensor had good selectivity for distinguishing different sequences of target miRNA.

3.5 Reproducibility and stability

The reproducibility of the sensor was researched by fabricating six sensors separately to detect 1.0 pM miRNA-21. The results showed that ΔR_{et} had a relative standard deviation of 4.2%, indicating that this sensor had good reproducibility. Additionally, this sensor was stored in Tris–HCl at 4 °C, and measurements were conducted once every day. After five days, we observed that the sensor could maintain about 98.9%, 97.5%, 96.8%, 92.6%, and 87.3% of its original response, which indicated that this sensor has sufficient stability for miRNA analysis.

3.6 Performance evaluation of miRNA detection

To evaluate the applicability and reliability of the sensor, different concentrations of miRNA-21 were spiked into 5% human serum samples obtained from a healthy individual. The recovery experiments were carried out, and acceptable recoveries of 96.0% and 97.0% were obtained (Table S3†).

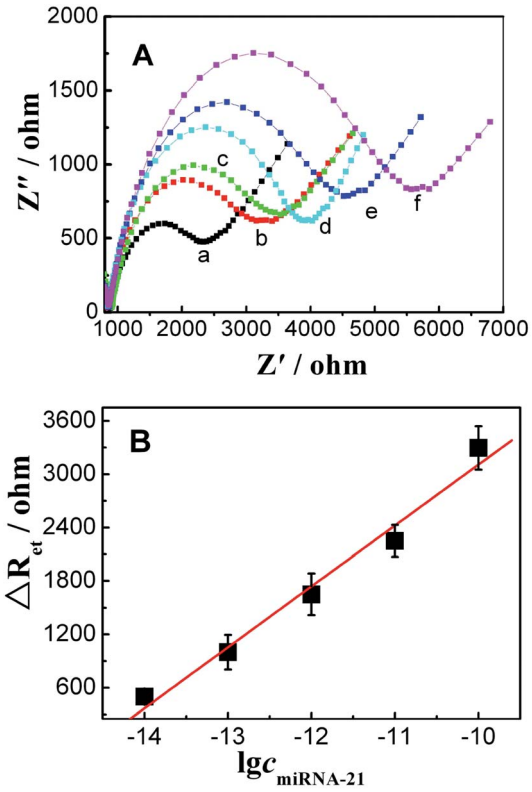

Fig. 4 (A) Impedance spectra of the sensor in Tris–HCl hybridization with different concentrations of miRNA-21: 0 (a), 1.0×10^{-14} (b), 1.0×10^{-13} (c), 1.0×10^{-12} (d), 1.0×10^{-11} (e), and 1.0×10^{-10} mol L^{-1} (f). (B) ΔR_{et} *vs.* the logarithm of the concentration of miRNA-21.

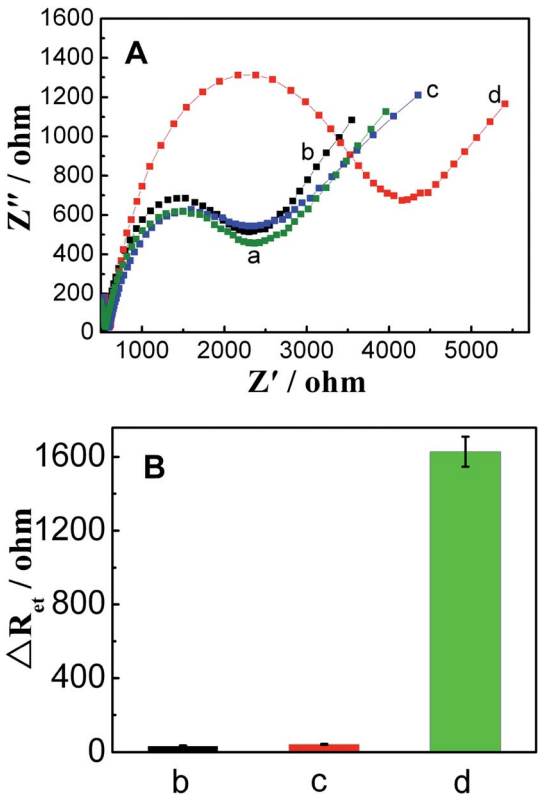

Fig. 5 (A) Impedance spectra of the sensor in Tris–HCl hybridization with different miRNA samples: blank (a), miRNA-141 (b), t-miRNA-21 (c), and miRNA-21 (d). (B) ΔR_{et} was obtained from (A). The concentration of miRNA-21: 1.0 pM, other RNAs: 0.1 nM.

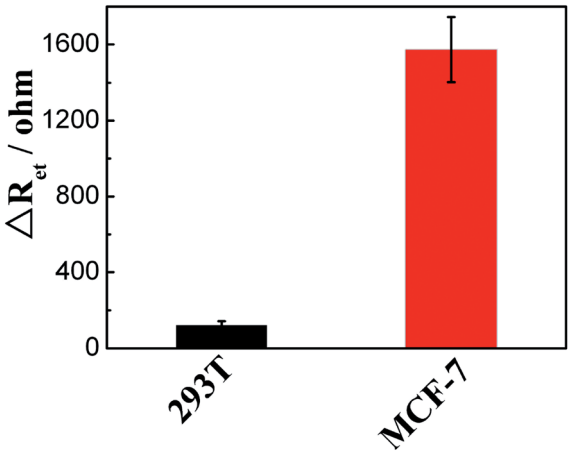

Fig. 6 ΔR_{et} for the detection of miRNA-21 extracted from 293T cells and MCF-7 cells.

Finally, this proposed sensor was applied to measure the expression levels of miRNA-21 in different cell lines using MCF-7 cells and human embryonic kidney cells (293T) as models. As shown in Fig. 6, ΔR_{et} obtained for incubation with the lysate from MCF-7 cells (10^4 cells) was much larger than that from 293T cells (10^4 cells), indicating that miRNA-21 was overexpressed in MCF-7 cells, which was in good agreement with the results of previous reports.[34,35]

4 Conclusions

In this study, an electrochemical impendence miRNA sensor based on ZrO_2-RGO/GCE is constructed. The catalytic hairpin assembly signal amplification strategy is used to improve the sensitivity of the sensor. The experiment results indicate that the sensor has effective selectivity to distinguish various target miRNAs. In addition, it displays good feasibility for detecting miRNA in human serum samples, and it can measure miRNA in real samples. This sensor provides a new method for detecting miRNA and has great potential in cancer diagnosis.

Conflicts of interest

There are no conflicts of interest to declare.

Acknowledgements

This project was supported by the Natural Science Research Key Project of Education Department of Anhui Province (KJ2017A434, KJ2016A888), the Opening Project of Anhui Key Laboratory of Spin Electron and Nanomaterials (2015YKF16), the Funded Project of Suzhou University Cultivate Outstanding Talent (SZXYQNL2017001) and Research Team of Anhui Provincial Education Department (2016SCXPTTD). Key Discipline of Material Science and Engineering of Suzhou University (2017XJZDXK3).

Notes and references

1 V. Benoit, A. Steel, M. Torres, Y. Y. Yu, H. J. Yang and J. Cooper, *Anal. Chem.*, 2001, **73**, 2412–2420.
2 S. Su, J. W. Fan, B. Xue, L. H. Yuwen, X. F. Liu, D. Pan, C. H. Fan and L. H. Wang, *ACS Appl. Mater. Interfaces*, 2014, **6**, 1152–1157.
3 A. R. Jilbert, *Meth. Mol. Biol.*, 2000, **123**, 177.
4 X. H. Yang, Q. Wang, K. M. Wang, W. H. Tan and H. M. Li, *Biosens. Bioelectron.*, 2007, **22**, 1106–1110.
5 T. Yang, M. J. Chen, Q. Q. Kong, X. L. Luo and K. Jiao, *Biosens. Bioelectron.*, 2017, **89**, 538–543.
6 H. Teymourian, A. Salimi and S. Khezrian, *Electroanalysis*, 2017, **29**, 409–414.
7 M. Chen, C. J. Hou, D. Q. Huo, H. B. Fa, Y. N. Zhao and C. H. Shen, *Sens. Actuators, B*, 2017, **239**, 421–429.
8 W. Wang, T. Bao, X. Zeng, H. Y. Xiong, W. Wen, X. H. Zhang and S. F. Wang, *Biosens. Bioelectron.*, 2017, **91**, 183–189.
9 S. Su, H. F. Sun, W. F. Cao, J. Chao, H. Z. Peng, X. L. Zuo, L. H. Yuwen, C. H. Fan and L. H. Wang, *ACS Appl. Mater. Interfaces*, 2016, **8**, 6826–6833.
10 J. Shu, Z. L. Qiu, S. Z. Lv, K. Y. Zhang and D. P. Tang, *Anal. Chem.*, 2018, **90**, 2425–2429.
11 Z. L. Qiu, J. Shu and D. P. Tang, *Anal. Chem.*, 2018, **90**, 1021–1028.
12 Z. L. Qiu, J. Shu and D. P. Tang, *Anal. Chem.*, 2017, **89**, 5152–5160.
13 T. Yang, Q. H. Li, L. Meng, X. H. Wang, W. W. Chen and K. Jiao, *ACS Appl. Mater. Interfaces*, 2013, **5**, 3495–3499.
14 Y. C. Yang, C. Li, L. Yin, M. Y. Liu, Z. X. Wang, Y. Q. Shu and G. X. Li, *ACS Appl. Mater. Interfaces*, 2014, **6**, 7579–7584.
15 K. Y. Zhang, S. Z. Lv, Z. Z. Lin, M. J. Li and D. P. Tang, *Biosens. Bioelectron.*, 2018, **101**, 159–166.
16 Q. Zhou, Y. X. Lin, K. Y. Zhang, M. J. Li and D. P. Tang, *Biosens. Bioelectron.*, 2018, **101**, 146–152.
17 J. Shu and D. P. Tang, *Chem.–Asian J.*, 2017, **12**, 2780–2789.
18 K. D. Dobson and A. J. McQuillan, *Langmuir*, 1997, **13**, 3392–3396.
19 M. Fang, D. M. Kaschak, A. C. Sutorik and T. E. Mallouk, *J. Am. Chem. Soc.*, 1997, **119**, 12184–12191.
20 S. Q. Liu, J. J. Xu and H. Y. Chen, *Bioelectrochemistry*, 2002, **57**, 149–154.
21 T. Yang, Y. Y. Feng, W. Zhang, S. Y. Ma and K. Jiao, *J. Electroanal. Chem.*, 2011, **656**, 140–146.
22 N. N. Zhu, A. P. Zhang, Q. J. Wang, P. G. He and Y. Z. Fang, *Anal. Chim. Acta*, 2004, **510**, 163–168.
23 Q. X. Wang, F. Gao, X. Zhang, B. Zhang, S. X. Li, Z. S. Hu and F. Gao, *Electrochim. Acta*, 2012, **62**, 250–255.
24 Y. H. Guo, J. Wu, J. Li and H. X. Ju, *Biosens. Bioelectron.*, 2016, **78**, 267–273.
25 Z. Wu, G. Q. Liu, X. L. Yang and J. H. Jiang, *J. Am. Chem. Soc.*, 2015, **137**, 6829–6836.
26 Y. Liu, T. Shen, J. Li, H. Gong, C. Y. Chen, X. M. Chen and C. Q. Cai, *ACS Sens.*, 2017, **2**, 1430–1434.
27 J. T. Liu, P. Du, J. Zhang, H. Shen and J. P. Lei, *Chem. Commun.*, 2018, **54**, 2550–2553.

28 Q. M. Feng, Y. H. Guo, J. J. Xu and H. Y. Chen, *ACS Appl. Mater. Interfaces*, 2017, **9**, 17637–17644.
29 X. Li, D. X. Li, W. J. Zhou, Y. Q. Chai, R. Yuan and Y. A. Xiang, *Chem. Commun.*, 2015, **51**, 11084–11087.
30 S. Thiagarajan, T. H. Tsai and S. M. Chen, *Biosens. Bioelectron.*, 2009, **24**, 2712–2715.
31 N. Zhang, K. Y. Zhang, Q. Wang, J. J. Xing and J. Chen, *Chin. J. Anal. Lab.*, 2014, **33**, 1413–1415.
32 G. Darabdhara, P. K. Boruah, P. Borthakur, N. Hussain, M. R. Das, T. Ahamad, S. M. Alshehri, V. Malgras, K. C. W. Wu and Y. Yamauchi, *Nanoscale*, 2016, **8**, 8276–8287.
33 P. K. Gupta, S. Tiwari, Z. H. Khan and P. R. Solanki, *J. Mater. Chem. B*, 2017, **5**, 2019–2033.
34 S. Li, L. G. Xu, W. Ma, X. l. Wu, M. Z. Sun, H. Kuang, L. B. Wang, N. A. Kotov and C. L. Xu, *J. Am. Chem. Soc.*, 2016, **138**, 306–312.
35 K. Y. Zhang, L. Yang, F. Lu, X. C. Wu and J. J. Zhu, *Small*, 2018, **14**, 1703858.